Research Progress in Mechanical and Manufacturing Engineering Vol. 4 No. 1 (2023) 504-517

RPMME

Homepage: http://penerbit.uthm.edu.my/periodicals/index.php/rpmme
e-ISSN : 2773-4765

Review On The Biosynthesis Of Composite TiO_2 - Inorganic/Metal Oxide (Fe_2O_3): Photocatalytic And Antibacterial Purpose Of Wastewater Treatment

Jaffner Anak Johngika[1], Zawati Harun[2]

[1]Universiti Tun Hussein Onn Malaysia, 86400, Parit Raja, Johor, MALAYSIA

[2]Advanced Manufacturing Material Centre (AMMC),
University Tun Hussein Onn Malaysia, 86400, Parit Raja, Johor, MALAYSIA

*Corresponding Author Designation

DOI: https://doi.org/10.30880/rpmme.2023.04.01.058
Received 15 July 2022; Accepted 26 January 2023; Available online 1 June 2023

Abstract: Photocatalytic process has the ability of to degrade or reduce toxicity substance by chemical reaction and producing non-hazardous gasses to the environment has attract many researchers to apply this technology in treating waste water problem recently. There are many methods to synthesize the composite TiO_2-Fe_2O_3, such as hydrothermal, sol-gel and ultrasonic impregnation methods, which will be described in this study for the comparison of which composite would have the highest rate of photocatalytic activity based on its synthesizing technique. In this research, the review of synthesized composite mixture of TiO_2-Fe_2O_3 will be investigated towards photocatalytic and antibacterial application. The analysis and comparison will be conducted based on phase analysis (XRD), Field Emission Scanning Electron Microscopy, FTIR analysis and UV–vis diffuse reflectance spectroscopy. Thus, the study will focus on the properties and performance analysis of composite inorganic particles in eliminating the mixture of organic pollution specifically for waste water treatment.

Keywords: Photocatalytic, Sol-gel, Synthesize, TiO_2-Fe_2O_3, Antibacterial Application, Phase Analysis (XRD), Field Emission Scanning Electron Microscopy, FTIR Analysis, UV–vis, Organic Pollution, Waste Water Treatment

1. Introduction

Recent technology has shown the potential of using nanoparticles from metal oxide and inorganic materials in degrading chemical substances such as dyes, oily waste, paint via photocatalytic process that has shown better effect towards conserving environment as its offer green technology approach. The ability of photocatalytic process to degrade or reduce toxicity substance by chemical reaction and producing non-hazardous gasses to the environment has attract many researchers to apply this technology in treating waste water problem recently (Ameta et al., 2018).

**Corresponding author: zawati@uthm.edu.my*

In this present work, the composite mixture between TiO_2 and Fe_2O_3 will be investigated towards photocatalytic and antibacterial application (Noh et al., 2016). Combination of this synthesized composite with biosynthesis technique will be considered as this will provide and offer much better green approach of waste water treatment by minimizing the toxic secondary waste product as well as minimizing the chemical usage in their synthesizing technique.

1.1 Significant of Study

The review will propose the most significant approach with a suitable processing-controlled parameter in producing composite TiO_2 and Fe_2O_3 nanoparticles that can perform effectively in photocatalytic process and as an antibacterial agent. It is also expected that the composite mixture of particles will show antibacterial properties and the synthesized of particles itself would offer an environmental-friendly technique, that satisfy the green-technology requirement.

2. Materials and Methods

There is various processing for synthesizing such as chemical and physical techniques may be used for manufacturing of TiO_2-Fe_2O_3 products such as sol-gel procedure, sonochemical system, electrochemical deposition, self-assembly caused by evaporation, atomic layer deposition (ALD), mechanochemical synthesis and techniques of hydrothermal production.

Since sol-gel method seems to be a promising method for synthesizing TiO_2-Fe_2O_3 with different properties and outcome for the best result of photocatalytic activity, it is safe to say that it is the best approach for this review of research papers.

2.1 Materials

Titanium dioxide (TiO_2) had already generally been known amongst the most effective photocatalysts for the reduction of environmental contamination as well as the generation of hydrogen through photocatalysis via water by sunlight irradiation. TiO_2 is ecologically safe and is therefore deemed to be a "green" catalyst. TiO_2 coatings tend to also have self-cleaning characteristics where TiO_2 reacts with the water whenever it is subjected to sunlight to produce hydroxyl radicals, that breaks down surface adsorbed organic molecules including bacteria (Dariani et al., 2016). Iron oxide would be a metal oxide transition that seems to have various stoichiometric as well as crystalline structures, along with wustite (FeO), hematite (Fe_2O_3), maghemite (v-Fe_2O_3), and magnetite (Fe_3O_4). This is a good potential photoelectrochemical (PEC) water separating photoanode substance. The photocatalytic efficiency of α-Fe_2O_3, however, remains restricted by conditions such as strong charge recombination for holes and electrons, short diffusion spans of holes (2-4 nm) including weak conductivity, leading to both weak efficiencies and greater requirements for photo-assisted water oxidation state (Singh et al., 2019). Inside the Ti sponge, the cause of oxygen toxicity is primarily the $TiOCl_2$ pollutant found in the raw resources, $TiCl_4$ (Song et al., 2014). Because $TiCl_4$ interacts towards humidity intensely which generates $TiOCl_2$ and HCl, as such an impurity, it often comprises several quantities of $TiOCl_2$. The $TiOCl_2$ material contained inside this $TiCl_4$ must be quantified, because $TiOCl_2$influences the consistency of the Ti sponge where oxygen has a major hardness effect. For its infrared characteristic spectrum line, $TiOCl_2$ can be measured by infrared spectroscopy. The weak alkali solution was also aqueous ammonia. Whenever it dissolves inside of an aqueous ammonia solution, CO2 reacts with both ammonia and hydroxyl ions. At temperatures from 5 to 50 C, the densities of ammonia solutions with dissimilar concentrations would be evaluated utilizing both an apycnometer as well as an Anton Paar Stabinger Viscometer SVM 3000 (Kang et al., 2019).

2.2 Methods

The nanocomposites were synthesised utilising 20 mL $TiOCl_2$, however in order to produce composites with different Fe-to-Ti ratios, each feed intake quantity of iron salts variedFe$Cl_3 \cdot 6H_2O$ and

$FeCl_2 \cdot 4H_2O$ ($Fe^{3+}:Fe^{2+} = 1:2$) had been initially applied and stirred at ambient temperature in distilled water. For all the synthesis tests, their ratio among Fe^{3+} and Fe^{2+} was held at 1:2. Table 2.1 provides the exact sum of $TiOCl_2$, $FeCl_3 \cdot 6H_2O$ and $FeCl_2 \cdot 4H_2O$ used throughout the synthesis of each specimen (Supporting information). The mixture was then applied to the $TiOCl_2$ solution in the beaker then mixed for 30 minutes (Abbas et al., 2016).

Its pH was about 1 and 2 of that initial solution consisting Ti and Fe precursors. Ammonia solution was then applied progressively. The final pH of 9 was retained. Slurry was aged for 4 hours at 80°C and then required to rest for 12 hours with soft stirring in ambient temperature. Throughout the oxidation of Fe_3O_4 to Fe_2O_3, ageing improves. This same product sample was treated with abundant amounts of ethanol and water. That powdered substance was dried for 24 hours in the 80°C thermal oven. That dried samples were then calcinated separately for 2 hours inside a box furnace for 3 various temperatures at 400°C, 600°C and 800°C to investigate the influence of the calcination temperature upon this property of the specimen. The heating rate was 5°C/minute and was heated in an atmospheric pressure environment. For the research of the impact of chemical proportions on the physical, morphological, optical and photochemical properties of binary oxide composite nanomaterials, the volume of Fe_2O_3 in TiO_2 was retained at 2%, 5%, 8 percent, 15%, 25% and 35% for various samples.

Table 2.1: TiO_2-Fe_2O_3 Composite's Structural and Textural Properties.

Sample name	Amount of Fe_2O_3 designed (wt%)	Amount of Fe_2O_3 by XRF (wt%)	Amount of TiO_2 by XRF (wt%)	Ti/Fe weight ratio by EDX	Crystallite size (nm)	Amount of rutile in TiO_2 (%)
Ti-600	0	0	100	-	21.5	-
TiFe2-600	2	2	98	82.8	14.5	-
TiFe5-600	5	5	95	33.6	11.8	-
TiFe8-600	8	8.11	91.89	18.6	14.5	-
TiFe15-600	15	15.1	84.9	10.5	12.7	-
TiFe25-600	25	25.5	74.5	5.1	30.7	36%
TiFe35-600	35	33.88	66.12	3.2	62.1	73%

For the 2, 5%, 8 percent, 15%, 25% and 35% Fe_2O_3 inside this composite matrix, those materials obtained were called TiFe2, TiFe5, TiFe8, TiFe15, TiFe25 and TiFe35. Iron salts are never applied to the $TiOCl_2$ solution to produce an un-doped pure titania. The remaining of the process will be exactly the same as synthesizing composites with TiFe. TiFeX-calcination temperature was called the calcined samples; whereby X is the Fe_2O_3's percentage inside this composite. For instance, TiO_2-Fe_2O_3 composite was designated as TiFe5-600 with 5wt percent Fe_2O_3 and calcinated at 600°C. Synthesized composites were labelled by adding '-As' that after specimen's name (Abbas et al., 2016)

X-ray diffraction (XRD) technology was used to analyze the crystal structure of the formulated TiO_2-Fe_2O_3 composites. Figure 2.2 shows the XRD-6000, Shimadzu X-ray Diffractor (Abbas et al., 2016). The field emission scanning electron microscopy machine analyzed the morphology of such materials collected under various conditions. In order to test the bonding pattern of such synthesized materials using the FTIR Spectrometer, Fourier transform infrared spectroscopy has been used for analysis. In order to characterize the presence of particular chemical groups in materials, FTIR spectroscopy is used. With FTIR spectroscopy, the structure of chemical reactions as well as the identification of unstable compounds are studied. A diffuse reflectance distribution (DRS) of a synthesised composite materials has been measured by the UV-Vis spectrophotometer. A particularly

useful technique to describe the local titanium atmosphere in titanosilicates is UV-vis diffuse reflectance spectroscopy (DRS). To contrast the photocatalytic behavior of TiO_2-Fe_2O_3 nanocomposites, a photochemical reaction for such removal of methylene blue was included. That depletion activity of methylene blue dye throughout the existence of TiO_2-Fe_2O_3 photocatalysts while irradiation was then reported as a feature of time in minute.

2.3 Results and Discussion

The analysis of titanium dioxide and iron (III) oxide, as well as the efficiency of Photocatalytic action, will be addressed in this section. And as per the previous study, experiment, and journal, the result is obtained. Numerous findings can also be correlated thanks to the experimental substance and treatment.

There were 7 authors chosen for comparison which is (Cheng et al., 2017), (Abbas et al., 2016), (Mirmasoomi et al., 2017), (M. Ahmadi Golsefidi *, F. Abbasi , M. Abrodi, Z. Abbasi, 2016), (Zhu et al., 2015), (Mohamed et al., 2017) and (Subramonian et al., 2017) which is using different synthesis method of hydrothermal, sol-gel, ultrasonic-assisted impregnation method, sonochemical-assisted method, electrochemical deposition, deposition-self-assembly technique and mechanochemical milling respectively. The purpose of this comparison is to gather different synthesis methods, come out with the best synthesis method and compare the varied parameters for the chosen methods with few other authors with the same method.

Research	**Technique**	**Targeted Characteristic for Comparison**
Author	**Method**	**Percentage of output synthesized**
(Cheng et al., 2017)	Hydrothermal	High
(Abbas et al., 2016)	Sol-gel	High
(Mirmasoomi et al., 2017)	Ultrasonic-assisted impregnation method	High
(M. Ahmadi Golsefidi *, F. Abbasi , M. Abrodi, Z. Abbasi, 2016)	Sonochemical-assisted method	Mediocre
(Zhu et al., 2015)	Electrochemical deposition	Moderate
(Mohamed et al., 2017)	Deposition-self assembly technique	Weak
(Subramonian et al., 2017)	Mechanochemical milling	High

Table 3.1 presents general comparison on different technique of composite TiO_2 synthesis. As can be observed from the table, the hydrothermal, Sol-gel, Ultrasonic-assisted impregnation method and Mechanochemical milling show the higher possibility in getting higher composite. Among this technique Sol-gel has reported the easiest, quick and good technique in synthesizing TiO_2 particles composite, as reported by other studies (Abbas et al., 2016). In fact, sol-gel also is one of the preferred techniques in synthesizing other inorganic particles since it gives better purity and more stable composite particles as reported elsewhere by the other researcher (Razani et al., 2017). Even though this technique involved chemical routes with higher toxicity materials but the potential output is quite

optimum with higher output possibility has made this technique to be used among researcher (Bouziani et al., 2020).

Table 3.2 presents specific comparison of composite TiO_2's synthesis. Although the level of purity of the composite is pure for all five of the authors, it may be comparable through the differences in temperature of calcination which may affect the result of the photocatalysis. In this case, the author: (Abbas et al., 2016), (Razani et al., 2017), (Bouziani et al., 2020), (Koohestani, 2019), and (Pang et al., 2016) has come out with different calcination temperature of 600, 550, 500, 450 and 200ºC respectively.

Table 3.2: Specific Comparison

Research	**Varied Parameters: Sol-Gel**	**Targeted Characteristic for Comparison**
Author	**Temperature, ºC (Calcination)**	**Level of Purity**
(Nadir Abbas, 2016)	600	Pure
(Afini Razani, 2017)	550	Pure
(Bouziani A, 2020)	500	Pure
(Hassan Koohestani, 2019)	450	Pure
(Yean Ling Pang, 2015)	200	Pure

Table 3.3 presents the method of Sol-Gel which explains briefly about the parameters, characteristic including performance. Each author has their own reaction or reduction medium used for their very own experiments.

Table 3.3: Methods Sol-Gel: Parameters/Characteristic/Performance

Research	**Vary Parameters (Significant)**		**Characteristic**		**Performance**
Author/ Year	**Temperature, ºC**	**Reaction/ Reduction Medium**	**Level of Purity**	**Particle Morphology**	**Band Gap**
(Abbas et al., 2016)	600	Titanium Oxychloride ($TiOCl_2$)	Pure	✓	✓
(Razani et al., 2017)	550	Ethanolic iron (III) nitrate nonahydrate with 0.1 mol/dm3 ethanolic titanium tert-butoxide solution	Pure	✓	✓
(Bouziani et al., 2020)	500	Iron III nitrate nonahydrate ($FeN_3O_9.9H_2O$), titanium tetra-isopropoxide (TTIP, 97%), acetic acid (CH_3COOH, 99.78%) and ethanol (C_2H_5OH, 99.5%)	Pure	✓	✓

(Koohestani, 2019)	450	Distilled water (85 cc), HCl (6 cc) and 2-propanol (6	Pure	✓	✓
(Pang et al., 2016)	200	$FeCl_2 \cdot 4H_2O$ and NaOH	Pure	✓	✓

The main focus for all of this comparison amongst the author would be the band gap for each of their published paper. The recorded data of parameters of TiO_2-Fe_2O_3 composites obtained from few journals entitled Sol–gel Synthesis of TiO_2-Fe_2O_3 Systems: Effects of Fe_2O_3 Content and Their Photocatalytic Properties (Abbas et al., 2016), Sol-Gel Synthesis of Fe_2O_3-Doped TiO_2 for Optimized Photocatalytic Degradation of 2,4-Dichlorophenoxyacetic Acid (Razani et al., 2017), Synthesis of α-Fe_2O_3/TiO_2 Heterogeneous Composites by the Sol-gel Process and Their Photocatalytic Activity (Bouziani et al., 2020), Synthesis and Characterisation of TiO_2 nanoparticles/Fe_2O_3 Waste Chips Composite (Koohestani, 2019), and Synthesis, Characteristics and Sonocatalytic Activities of Calcined γ-TiO_2 and TiO_2 Nanotubes/ γ-TiO_2 Magnetic Catalysts in the Degradation of Orange G (Pang et al., 2016).

3.2 Photocatalytic Activity

3.2.1 Based on 600ºC's Calcination Temperature

Figure 3.1 shows the deterioration of methylene blue dye throughout the presence of Ti-600, TiFe5-400, TiFe2-600, TiFe5-600, TiFe8-600, TiFe15-600, TiFe25-600, and TiFe35-600 photocatalysts as a time - dependent (min). It also demonstrates that all composite materials that have been produced have photocatalytic properties. Its reaction prepared by the addition of TiFe5-600 catalyst yielded the most methylene blue deterioration. Amongst these developed setups, TiFe8-600 was the second most successful catalyst. TiFe15-600, TiFe25-600, and TiFe35-600 have considerably lower photocatalytic effectiveness than TiFe5 and TiFe8. TiFe5, a substance containing 5% Fe2O3 doping in TiO2, has been discovered to be the best catalyst compound amongst other. Figure 3.1 shows the deterioration curve for TiFe5-400 to show the influence of calcination temperature. TiFe5-400 likewise shown high degrading efficiency; however, TiFe5-600 photocatalytic performance was found to be superior than TiFe5-400's.

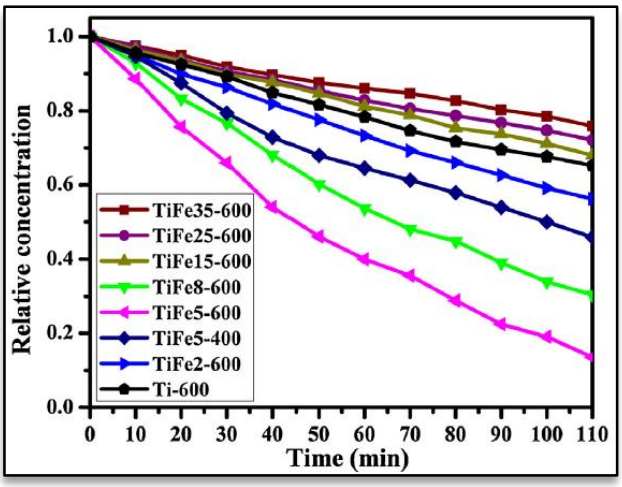

Figure 3.1: The Degradation of Methylene Blue Dye Solution by Photocatalysis

Figure 3.2 illustrates the plot of reaction time versus the logarithms of relative concentration of methylene blue dye solution ($\ln C_0/C$). By all trials, the trends demonstrate a linear relationship between methylene blue dye solution and response time. Their reaction rate changes for each sample,

demonstrating that perhaps the catalytic activity for powdered materials is highly influenced by a variety of structural and chemical compositional characteristics. The reaction rates of 15%, 25%, and 35% iron oxide comprising catalysts were lower than the rate constants of 5% and 8% iron oxide comprising catalysts. The TiFe5 specimen had the greatest rate constant.

Each alteration in photocatalytic activity with Fe_2O_3 content proves that such quantity of Fe_2O_3 in blended oxides influences the crystallinity, particle size, porosity, and optical properties of TiO_2-Fe_2O_3 composites, which in turn affects the crystallinity, particle size, porosity, and optical properties of TiO_2-Fe_2O_3 composites. According to photocatalytic studies, the proportion of methylene blue dye adsorbed on catalyst surface was measured in adsorption–desorption equilibrium investigations. The greatest adsorption was found in TiFe5-600 and TiFe8-600, with 27% and 29%, respectively. Methylene blue dye adsorption was found to be 23%, 24%, 21%, 22%, and 24% on Ti-600, TiFe2-600, TiFe15-600, TiFe25-600, and TiFe35-600, respectively.

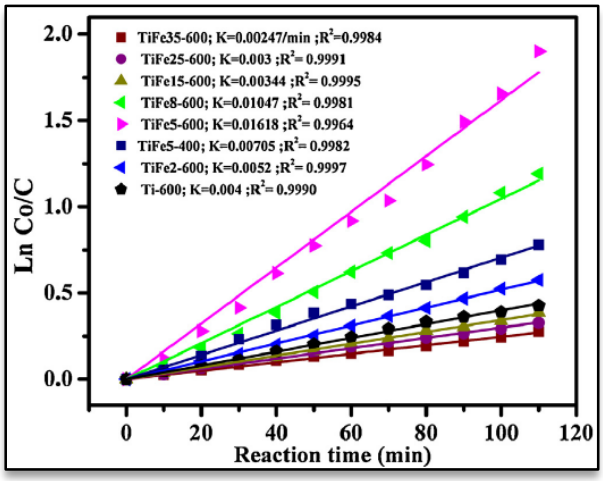

Figure 3.2: Linear Relationship Between Reaction Time and Logarithm of Relative Methylene Blue Concentration

3.2.2 Based on 550ºC's Calcination Temperature

The efficiency of Fe_2O_3-doped and undoped TiO_2 photocatalysts was tested, and thus the results are shown in Figure 3.3. Figure 3.4 shows the gradual degradation of 2,4-Dichlorophenoxyacetic acid by 0.05wt% Fe_2O_3 doped TiO_2 as a factor of irradiation time.

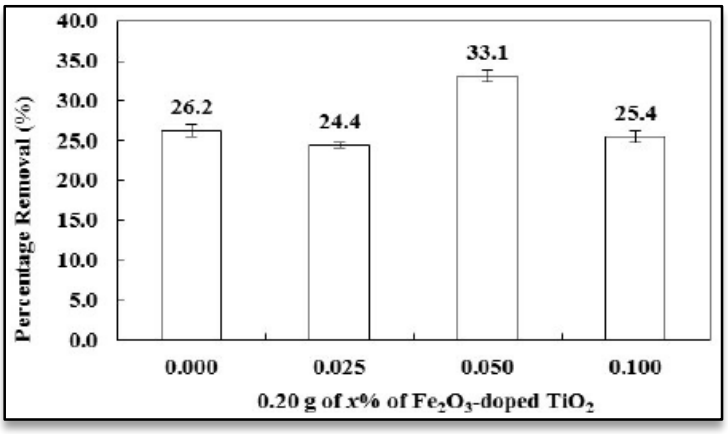

Figure 3.3: Percentage of 10 ppm 2,4-Dichlorophenoxyacetic Acid Degradation Using a 0.2 g/L Catalyst at pH 4.7.

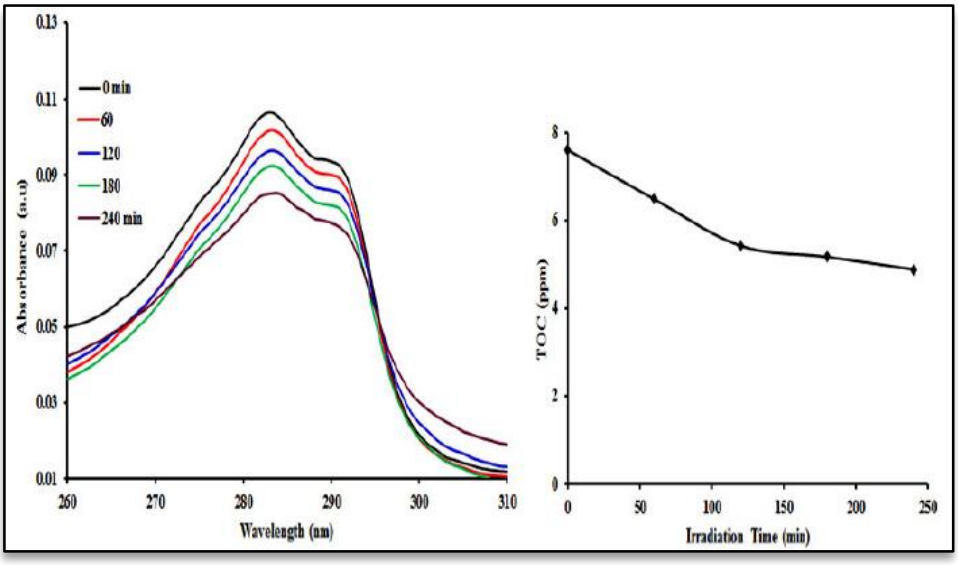

Figure 3.4: The Gradual Degradation of 2,4-Dichlorophenoxyacetic Acid as a Function of Irradiation Time Monitored via UV-vis Spectra and TOC Analysis

The Fe^{3+}ion, which functions as shallow trapping points for charge carriers and therefore separates the time of arrival of e^+ and h^+ couples to the catalyst surface, could be due to the increased photo catalytic activity reported for the 0.05wt% Fe_2O_3 doped TiO_2. Meanwhile, the Fe^{3+}ion prevents photo-generated e^- and h^+ couples from recombining. The photo produced electron being trapped increases the usage efficiency of the photo generated e^- and h^+ couples by doping TiO_2 with an appropriate Fe^{3+}ion concentration. Greater Fe^{3+} dopant concentrations could function as recombination sites for photo-generated e^- and h^+ couples, lowering photo catalytic activity.

3.2.3 Based on 500ºC's Calcination Temperature

Figure 3.5 depicts the absorption and photodegradation operations for the methylene blue solution which contains α-Fe_2O_3 particles calcined at various temperatures in dark and sun-like light, respectively. Methylene blue absorption and photodegradation were found to be low in α-Fe_2O_3 particles in experiments (3% and 8%, respectively).

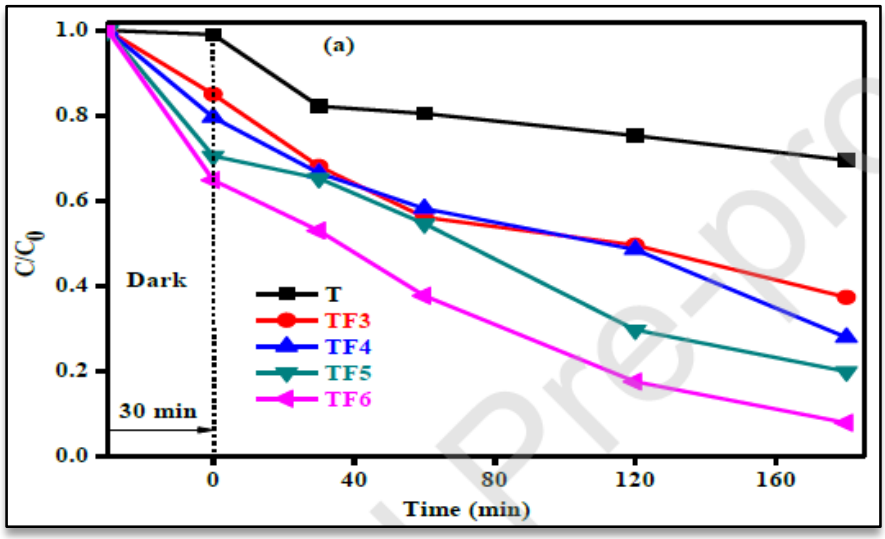

Figure 3.5: Conversion Plots for Photochemical Discoloration

Experimental conversion plots of methylene blue and phenol for the produced pristine TiO_2 powder are shown in Figure 3.6. After 180 minutes of sun-like light, both methylene blue and phenol show less than 30% conversion. While the calcination temperature of α-Fe_2O_3 powder increased, the photoactivity of that same composites increased. After 120 minutes of illumination, the greatest degradation rate for both methylene blue (92%) and Ph (52%) was observed for TF6.

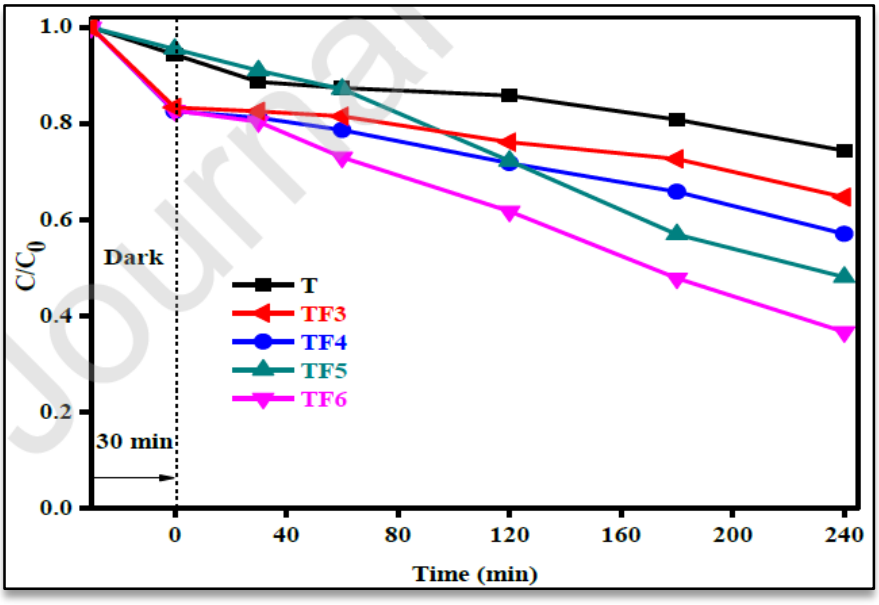

Figure 3.6: Conversion Plots for Photodegradation of Ph Under Sun-like Illumination.

Via first order rate kinetics, the reaction rates involving methylene blue and phenol for the chosen powders were determined. Table 3.9 summarizes the findings. The reaction rates appear to rise when α-Fe_2O_3 is integrated into TiO_2, as well as as the calcination temperature of α-Fe_2O_3 is raised. With both absorbents, an increase in TiO_2 photoactivity was found. By either methylene blue or phenol, its greatest photoactivity were achieved using TF6 composite. Regarding methylene blue and phenol, the photocatalytic reaction rates of the TF6 composite were 0.12 and 0.004 min^{-1}, respectively. Better crystallinity and successful interfacial contacts of α-Fe_2O_3 and TiO_2 are credited for the enhanced photocatalytic reaction rates. Each photodegradation pace of methylene blue and phenol was similarly impacted by the calcination temperature of a pristine α-Fe_2O_3 powder. Because the calcination temperature of a pristine α-Fe_2O_3 powder was raised, the photoactivity of the α-Fe_2O_3/TiO_2composites improves. The findings back up the enhancement in crystallite size described earlier in this paper. Following 120 minutes of irradiation, the TF6 composites represents the highest photodegradation for both methylene blue (92%) and phenol (52%). That enhancement is due to improved visible light absorption efficiency, which leads to the production of photo-generated electrons enabling effective charge separation.

Table 3.9: Reaction Rates for Methylene Blue and Phenol for the Selected Powders.

Powder	K (min^{-1})	
	Methylene Blue	Phenol
T	0.0023	0.001
TF3	0.0045	0.0013
TF4	0.0056	0.0018

TF5	0.0076	0.0028
TF6	0.012	0.004

3.2.4 Based on 450ºC's Calcination Temperature

Methylene orange is a model contaminant for photocatalytic degradation processes and is harmful to marine life. Figure 3.7 shows the deterioration of methylene orange pigment throughout the presence of TiO_2 and TiO_2/Fe_2O_3 mixtures as a function of frequency during irradiation. The inclusion of TiO_2 improved photocatalytic efficiency since pure TiO_2 only destroyed 74% of methylene orange in such a time period of 180 minutes, whereas Fe_2O_3 increased performance. The highest degrading efficiency was achieved when the operation was conducted out throughout the presence of TiO_2–10% Fe_2O_3, following whereby the efficiency decreased when the Fe_2O_3 percentage was increased.

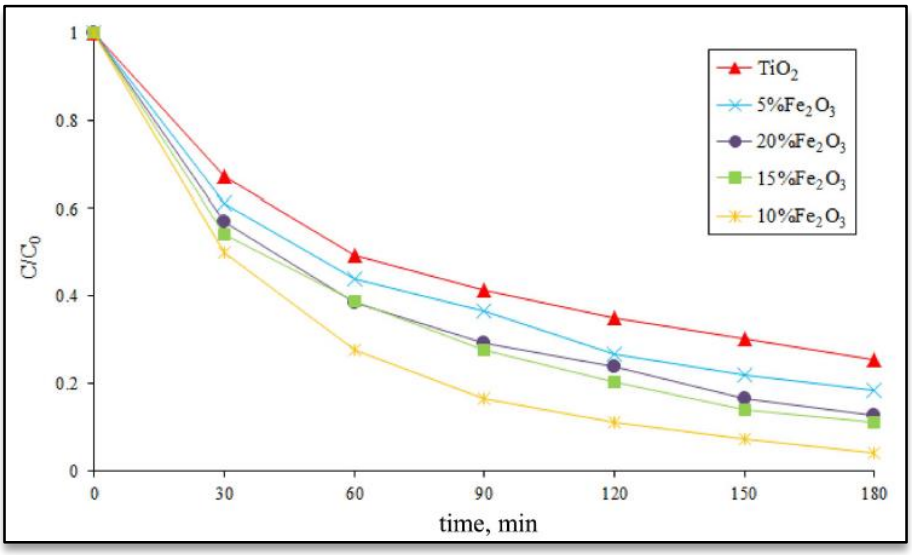

Figure 3.7: Degradation of Methylene Orange

TiO_2-10%Fe_2O_3 induced the most significant decrease of methylene orange, which was 96%. Upon 180 minutes of response time, the elimination data were acquired by UV–Vis and TOC analyses are listed in Table 3.10. TiO_2-10%Fe_2O_3 had the highest performance for methylene orange's deterioration under the same parameters.

Table 3.10: Removal Results Obtained by UV–Vis and TOC Measurements After the Reaction Time

Samples	UV–Vis,%	Rate constant, min^{-1}
TiO_2	74	0.0084
TiO_2-5%Fe_2O_3	82	0.0103
TiO_2-10%Fe_2O_3	96	0.0182
TiO_2-15%Fe_2O_3	89	0.0131
TiO_2-20%Fe_2O_3	87	0.0121

3.2.5 Based on 200ºC's Calcination Temperature

Table 3.11 shows that such calcination temperature as well as the inclusion of TiO_2 NTs inside this composite had an impact upon that specific surface area as well as mesoporous volume. As that the calcination temperature rises, the amount of porosity throughout the calcined γ-Fe_2O_3 sample reduced. Because tiny holes collapsed, its porosity volume decreased, indicating a development of big pores. Because of the decreased porosity, fewer nitrogen gas may be adsorbed upon that catalyst surface, resulting in a reduction on contact area. Its specific surface area dropped from 26.15 to 10.48 m^2/g because as calcination temperature increased from 200 to 500°C, revealing that calcination of 500°C resulted in substantial material growth. Once the weight ratio of TiO_2 NTs/γ-Fe_2O_3 composites were raised from 1:5 to 10:1, the total area of γ-Fe_2O_3 rose from 49.55 to 181.51 m^2/g. Because γ-Fe_2O_3 calcined at 200°C seems to have a modest surface area and mesoporous volume (26.15 m^2/g and 0.093 cm^3/g, respectively), its inclusion throughout composites should result in a reduction in surface area as well as mesoporous volume compared to that of pure TiO_2 NTs.

Table 4.11: Catalytic properties of the calcined γ-Fe_2O_3 at various calcination temperatures and TiO_2 NTs/γ-Fe_2O_3 composites at various compositions.

Samples	Indirect Band Gap Energy (eV)
γ-$Fe_2O_3$100	1.90
γ-$Fe_2O_3$200	1.99
γ-$Fe_2O_3$300	1.75
γ-$Fe_2O_3$500	1.85
Ti: Fe = 1: 5	2.80
Ti: Fe = 1: 1	2.85
Ti: Fe = 5: 1	3.02
Ti: Fe = 10: 1	3.05
TiO_2 NTs	3.08

3.3 Comparison Amongst Catalyst by Different Author

All of their composite as a catalyst proves that photocatalysis can be done with their produced specimens which they proven that they have their own best specimens to prove it was a success. Therefore, as a review, the comparison amongst each author's best specimen would be differentiate accordingly with prove that supports the statement. The Specimen for each of the author's best product of catalyst is shown in Table 3.12.

Table 4.12: Best Specimens by Each Authors

Author	Calcination Temperature (°C)	Best Specimen	Band Gap Energy (eV)
(Abbas et al., 2016)	600	TiFe25-600	1.87
(Razani et al., 2017)	550	0.025%$Fe_2O_3 - TiO_2$	3.10
(Bouziani et al., 2020)	500	TF5	2.62

(Koohestani, 2019)	450	TiO_2-10%Fe_2O_3	2.72
(Pang et al., 2016)	200	Ti: Fe = 10: 1	3.05

For the specimen done by calcination temperature of 600°C (Abbas et al., 2016), In TiO_2-Fe_2O_3 nanocomposites, a 5% incorporation of Fe_2O_3 into TiO_2 is determined to become the optimal quantity for morphological and photocatalytic benefits. When compared with Ti-600, BET research revealed that TiFe5-600 has a higher surface area. Owing to its excellent characteristics, the TiFe5-600 sample had the greatest photocatalytic activity amongst those produced materials.

Calcination temperature that was done at 550°C (Razani et al., 2017), an optimal quantity of Fe_2O_3 which can be incorporated into TiO_2 photocatalyst to generate the greatest 2,4-DA elimination is 0.05 wt percent. With 10 ppm 2,4-DA solution, 1.0 g of 0.05wt% Fe_2O_3 doped TiO_2, plus pH 4, the optimal elimination of 48.64% was estimated using response surface techniques. At the temperature of 500°C for the calcination(Bouziani et al., 2020), during sun-like light, the α-Fe_2O_3 /TiO_2 composites demonstrate improved photocatalytic activity to destroy both methylene blue and phenol. As when the calcination temperature of such pristine α-Fe_2O_3 powder is elevated, these photoactivity of such α-Fe_2O_3 /TiO_2 mixtures for the photodegradation frequency of MB and Ph enhances as well.

When the temperature of the calcination is 450°C (Koohestani, 2019), This impact of Fe_2O_3 composition on methylene orange decolorization was investigated, and it was discovered that the higher the Fe_2O_3 concentration, the faster the methylene orange decolorization rate. As for the specimen that was calcined at 200°C (Pang et al., 2016), the sonocatalytic characteristics, stability, and magnetic separability so that as-synthesised TiO_2 NTs/γ-Fe_2O_3 composites are all good. Although, to make it excellent at achieving its band gap, the ratio for TiO_2 are required to be bigger than γ-Fe_2O_3 which therefore are quite obsolete as to be compared with the rest of the author. Based on the information discovered by those authors, the discovery is consistent with a recent research, where found that the sample containing 7 wt% Fe_2O_3 in TiO_2-Fe_2O_3 combinations had the best photocatalytic activity. The photocatalytic activity of TiFe5-600 was considered to be effective than TiFe5-400 (Abbas et al., 2016). Due to its limited oxidation capability, the semiconductor with a narrow band gap energy displayed low visible light photocatalytic performance (Pang et al., 2016). It is yet to be decided that the best method for this experiment is to have a calcination temperature 550°C and the amount of 0.025%Fe_2O_3 for a good catalyst.

4. Conclusion

The sol-gel method was successfully done to combine both catalysts into a desired photocatalyst with different properties as done by all five researchers. The inclusion of such an adequate quantity of Fe_2O_3 improves the crystalline structure morphology, surface area, porosity, and eventually photocatalytic activity as per according to research. Based on the results obtained by each author, different approach can be used to conduct the photocatalysis experiments. It is observed that when Fe_2O_3 were to be calcined at a high temperature around 550°C, the amount of calcined Fe_2O_3 should be around 0.025% to be synthesized with TiO_2 for an optimum and efficient catalyst. However, the biosynthesis of TiO_2-Fe_2O_3 can still be improve for a better catalyst for wastewater treatment in the future. For example, Higher temperature up until 550°C shall be used to calcine Fe_2O_3 at the optimum amount at around 0.025%wt before synthesized with TiO_2 for the best result of photocatalysis because when calcination temperature reaches 600°C or more, it tend to deteriorate the quality of the catalyst. Other than that, as the temperature of the calcination reduce, the amount of Fe_2O_3 shall be increase as done by one of the authors which uses 450°C and applying the amount of 10%wt Fe_2O_3 which absorb the most contaminants in the experiments. It is also important that when calcination temperature was decided to be lower such as one of the authors where uses the

temperature of 200°C, the ratio of TiO_2 to Fe_2O_3 shall be bigger for TiO_2 to produce the best and efficient catalyst.

Acknowledgement

The authors wish to thank to the Faculty of Mechanical and Manufacturing Engineering, Universiti Tun Hussein Onn Malaysia that has supported on the accomplishment of research activity.

References

[1] Abbas, N., Shao, G. N., Haider, M. S., Imran, S. M., Park, S. S., & Kim, H. T. (2016). Sol–gel synthesis of TiO2-Fe2O3 systems: Effects of Fe2O3 content and their photocatalytic properties. *Journal of Industrial and Engineering Chemistry*, *39*, 112–120. https://doi.org/10.1016/j.jiec.2016.05.015

[2] Ameta, R., Solanki, M. S., Benjamin, S., & Ameta, S. C. (2018). Photocatalysis. In *Advanced Oxidation Processes for Wastewater Treatment: Emerging Green Chemical Technology*. https://doi.org/10.1016/B978-0-12-810499-6.00006-1

[3] Bouziani, A., Park, J., & Ozturk, A. (2020). Synthesis of α-Fe2O3/TiO2 heterogeneous composites by the sol-gel process and their photocatalytic activity. *Journal of Photochemistry and Photobiology A: Chemistry*, *400*, 112718. https://doi.org/10.1016/j.jphotochem.2020.112718

[4] Cheng, G., Xu, F., Xiong, J., Wei, Y., Stadler, F. J., & Chen, R. (2017). A novel protocol to design TiO2-Fe2O3 hybrids with effective charge separation efficiency for improved photocatalysis. *Advanced Powder Technology*, *28*(2), 665–670. https://doi.org/10.1016/j.apt.2016.12.004

[5] Dariani, R. S., Esmaeili, A., Mortezaali, A., & Dehghanpour, S. (2016). Photocatalytic reaction and degradation of methylene blue on TiO2 nano-sized particles. *Optik*. https://doi.org/10.1016/j.ijleo.2016.04.026

[6] Kang, X., Liu, S., Dai, Z., He, Y., Song, X., & Tan, Z. (2019). Titanium dioxide: From engineering to applications. In *Catalysts* (Vol. 9, Issue 2). https://doi.org/10.3390/catal9020191

[7] Koohestani, H. (2019). Synthesis and characterisation of TiO2 nanoparticles/Fe2O3 waste chips composite. *Micro and Nano Letters*, *14*(6), 678–682. https://doi.org/10.1049/mnl.2018.5583

[8] M. Ahmadi Golsefidi *, F. Abbasi , M. Abrodi, Z. Abbasi, F. yazarlou. (2016). Synthesis, Characterization and Photocatalytic Activity of Fe2O3 -TiO2 Nanoparticles and Nanocomposites. *J. Nanostructure*, *6*(1), 64–69. https://doi.org/10.7508/jns.2016.01.010

[9] Mirmasoomi, S. R., Mehdipour Ghazi, M., & Galedari, M. (2017). Photocatalytic degradation of diazinon under visible light using TiO2/Fe2O3nanocomposite synthesized by ultrasonic-assisted impregnation method. *Separation and Purification Technology*, *175*, 418–427. https://doi.org/10.1016/j.seppur.2016.11.021

[10] Mohamed, M. M., Bayoumy, W. A., Goher, M. E., Abdo, M. H., & Mansour El-Ashkar, T. Y. (2017). Optimization of α-Fe 2 O 3 @Fe 3 O 4 incorporated N-TiO 2 as super effective photocatalysts under visible light irradiation. *Applied Surface Science*, *412*, 668–682. https://doi.org/10.1016/j.apsusc.2017.03.200

[11] Noh, J., Yi, M., Hwang, S., Im, K. M., Yu, T., & Kim, J. (2016). A facile synthesis of rutile-rich titanium oxide nanoparticles using reverse micelle method and their photocatalytic applications. *Journal of Industrial and Engineering Chemistry*, *33*, 369–373. https://doi.org/10.1016/j.jiec.2015.10.020

[12] Pang, Y. L., Lim, S., Ong, H. C., & Chong, W. T. (2016). Synthesis, characteristics and sonocatalytic activities of calcined γ-Fe2O3 and TiO2 nanotubes/γ-Fe2O3 magnetic catalysts in

the degradation of Orange G. *Ultrasonics Sonochemistry*, *29*, 317–327. https://doi.org/10.1016/j.ultsonch.2015.10.003

[13] Razani, A., Abdullah, A. H., Fitrianto, A., Yusof, N. A., & Gaya, U. I. (2017). Sol-gel synthesis of Fe2O3-doped TiO2 for optimized photocatalytic degradation of 2,4- dichlorophenoxyacetic acid. *Oriental Journal of Chemistry*, *33*(4), 1959–1968. https://doi.org/10.13005/ojc/330442

[14] Singh, P., Sharma, K., Hasija, V., Sharma, V., Sharma, S., Raizada, P., Singh, M., Saini, A. K., Hosseini-Bandegharaei, A., & Thakur, V. K. (2019). Systematic review on applicability of magnetic iron oxides–integrated photocatalysts for degradation of organic pollutants in water. *Materials Today Chemistry*, *14*, 100186. https://doi.org/10.1016/j.mtchem.2019.08.005

[15] Song, G. L., Luo, Y. J., Li, J. Q., Li, Z. Bin, & Tan, H. (2014). Determination of titanium oxychloride in refined titanium tetrachloride by infrared spectroscopy. *Advanced Materials Research*, *997*, 475–479. https://doi.org/10.4028/www.scientific.net/AMR.997.475

[16] Subramonian, W., Wu, T. Y., & Chai, S. P. (2017). Photocatalytic degradation of industrial pulp and paper mill effluent using synthesized magnetic Fe2O3-TiO2: Treatment efficiency and characterizations of reused photocatalyst. *Journal of Environmental Management*, *187*, 298–310. https://doi.org/10.1016/j.jenvman.2016.10.024

[17] Zhu, X., Cui, X., Che, Z., Jin, X., & Li, M. (2015). Thermal decomposition fabrication of Fe2O3 nanoparticle-sensitized TiO2 nanotube arrays and their photoelectrochemical properties. *Journal of Nanoscience and Nanotechnology*, *15*(12), 9717–9720. https://doi.org/10.1166/jnn.2015.10310